JCTC Journal of Chemical Theory and Computation

Article

pubs.acs.org/JCTC

Molecular Dynamics Simulations of a Characteristic DPC Micelle in Water

Stéphane Abel,*[,†] François-Yves Dupradeau,[‡] and Massimo Marchi[†]

[†]Commissariat à l'Energie Atomique et aux Energies Alternatives, DSV/iBiTEC-S/SB2SM/LBMS, Saclay, France, CNRS UMR 8221, Saclay, France

[‡]Laboratoire des glucides, UFR de Pharmacie & CNRS FRE 3517, Université de Picardie-Jules Verne, Amiens, France

Supporting Information

ABSTRACT: We present the first comparative molecular dynamics investigation for a dodecylphosphocholine (DPC) micelle performed in condensed phase using the CHARMM36, GROMOS53A6, GROMOS54A7, and GROMOS53A6/Berger force fields and a set of parameters developed anew. Our potential consists of newly derived RESP atomic charges, which are associated with the Amber99SB force field developed for proteins. This new potential is expressly designed for simulations of peptides and transmembrane proteins in a micellar environment. To validate this new ensemble, molecular dynamics simulations of a DPC micelle composed of 54 monomers were carried out in explicit water using a "self-assembling" approach. Characteristic micellar properties such as aggregation kinetic, volume, size, shape, surface area, internal structure, surfactant conformation, and hydration were thoroughly examined and compared with experiments. Derived RESP charge values combined with parameters taken from Amber99SB reproduce reasonably well important structural properties and experimental data compared to the other tested force fields. However, the headgroup and alkyl chain conformations or the micelle hydration simulated with the Amber99SB force field display some differences. In particular, we show that Amber99SB slightly overestimates the trans population of the alkyl $Csp^3-Csp^3-Csp^3-Csp^3$ dihedral angle (i.e., CCCC) and reduces the flexibility of the DPC alkyl chain. In agreement with experiments and previously published studies, the DPC micelle shows a slightly ellipsoidal shape with a radius of gyration of ∼17 Å for the different potentials evaluated. The surface of contact between the DPC headgroup and water molecules represents between 70% and 80% of the total micelle surface independently of the force field considered. Finally, molecular dynamics simulations show that water molecules form various hydrogen-bond patterns with the surfactant headgroup, as noted previously for phospholipids with a phosphatidylcholine headgroup.

I. INTRODUCTION

Membrane proteins (MPs) are amphiphilic in nature. As such, to be manipulated and studied in aqueous solution and to remain biologically active, MPs have to be transferred in a suitable membrane-mimicking environment such as a detergent solution. Unfortunately, there is no systematic way for identifying the ideal detergent for a given MP, and empirical criteria are often used in this effort. Among the large variety of detergents available for purifying MPs,[1−4] dodecylphosphocholine (DPC, Figure 1) is considered to be a good mimicking system for eukaryotic membranes and is widely used to study the structure of purified transmembrane peptides and MPs (see, for instance, refs 5−11 and recent reviews[12,13]).

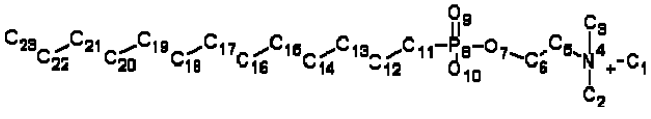

Figure 1. DPC surfactant with the atom-numbering scheme used in this work. Hydrogen atoms are omitted for clarity.

Structural and dynamical properties of DPC micelles have been extensively studied in the past using different experimental methods[5,6,10,14,15] as well as molecular dynamics (MD) simulations in explicit[8,16−22] or implicit[23] solvents. Although these works provide a large amount of data for validating new force fields, no systematic MD comparative study involving recent force fields available in popular suites of programs has been attempted for DPC micelles so far. Thus, the first motivation of this work was to investigate the structural and dynamical properties of a characteristic DPC micelle with a new potential compatible with the Amber99SB force field and validate the ensemble against popular biomolecular force fields.

Here, we report on derivation and validation of a new set of restrained electrostatic potential (RESP) charges for DPC developed using the "building blocks" approach[24,25] to be used for transmembrane peptides and MPs in a micellar environment.[26] To the best of our knowledge, the Amber99SB force field, in contrast to others (e.g., CHARMM or GROMOS), does not provide any specific parameter set for detergent molecules with phosphocholine headgroup. Testing the Amber99SB force field,[27] widely used to model proteins, in the context of detergents can be particularly useful. Recently, several new parameters for various membrane phospholipids compatible with the AMBER force field (such as AMBER99 or AMBER03) and the general Amber force field (GAFF) were published in the literature.[28−32] To develop their force fields, the authors used a "whole molecule" approach and different phospholipid conformations were extracted from bilayer

Received: April 22, 2012
Published: August 24, 2012

simulations to derive RESP charges values. This approach significantly differs from the approach used in this work where RESP charges of DPC are derived from building blocks (see below). Additionally, in the work of Jämbeck and Lyubartsev,[28,29] the authors mixed in their force fields bonded parameters directly taken from the CHARMM36 force[33] and added the Urey–Bradley bonding term not available in the AMBER energy function and not implemented in the *pmemd* and *Sander* MD codes. As a consequence, these new potentials are not directly transferable for studying phospholipid-based surfactants by MD simulations programs.

As underlined above, to derive the RESP atomic charge values for DPC the detergent molecule was split into elementary functional groups. In the past, we successfully employed this approach to derive partial charges for alkylglycoside surfactants and build a new set of force field libraries[34] compatible with the GLYCAM force field.[35] In the present study, the theory level used is chosen to be compatible with the Amber99SB force field (see next section).[27,36−38] Atomic charge values were validated by performing MD simulations for a micelle constituted of 54 DPC monomers in explicit TIP3P water molecules with force field parameters taken from Amber99SB.[27] The capital letter atom types used for proteins and defined in the Cornell et al. force field were also used for DPC, leading to a simple and homogeneous approach. Thus, the different organic functions present in DPC can be directly handled by the Amber99SB force field. GAFF was not used in this work.[32,38] Use of its lower case atom types would have added complexity to the molecular system. Indeed, force field parameters for DPC taken from Amber99SB and GAFF present important similarities. Nevertheless, it is strongly recommended to use homogeneous and consistent parameters in a simulation to model a heterogeneous molecular system such as a protein embedded in detergent molecules, thus extending the applicability of Amber99SB (or the last version of the Amber force field for proteins). It is also advised against mixing different force fields.[39,40]

This paper is organized as follows: the procedure used to derive the RESP atomic charges for DPC within the AMBER framework is first presented, and then sections covering MD simulations, the corresponding results, and their interpretations are discussed.

II. METHODS

II.1. RESP Charge Derivation for DPC. RESP charge derivation for DPC was carried out by following the approach previously described[41,42] and using rigorously defined building blocks.[35,36] This approach has many advantages over the whole molecule approach: (i) the computational time required for geometry optimization and molecular electrostatic potential (MEP) computation is drastically decreased, (ii) the optimized geometry of the conformation(s) of each building block is fully defined and controlled, (iii) optimized conformations presenting intramolecular hydrogen bonds are discarded from charge derivation to avoid overpolarization effects, and finally (iv) a large set of analog molecules can be simultaneously involved in charge derivation leading to a homogeneous Force Field Topology DataBase (FFTopDB) (see, for instance, the "F-72", "F-85", and "F-87" projects in the RESP ESP charge DDataBase (R.E.DD.B.) at http://q4md-forcefieldtools.org/REDDB/).[43] Molecule DPC was split into three elementary building blocks, choline, ethylmethylphosphate, and 1-dodecanol (Figure 2), to avoid unwanted nonbonded interactions between the charged

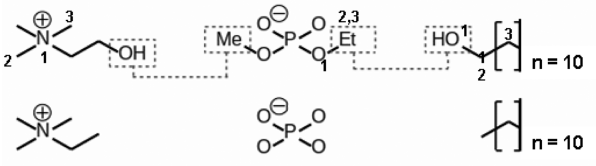

Figure 2. Building block scheme used to derive the RESP charges for DPC molecule. RESP charge values, force field libraries, as well as optimized geometries were submitted in the R.E.DDB database and are available under the "F-92" R.E.DD.B code. "Et" and "Me" stand for the ethyl and methyl groups, respectively. Note that nitrogen and carbon atoms in the upper figures were numbered according to the RESP charge derivation procedure described in the main text. Intermolecular charge constraints used during the fitting step are represented using dashed boxes and lines (see the main text for details). This allows defining the molecular fragments required for construction of the DPC surfactant.

groups of DPC observed during geometry optimization in the gas phase. For each building block the lowest minimum found after conformational search was involved in charge derivation. Thus, choline and 1-dodecanol molecular structures were constructed in their extended conformation. Ethyl methyl phosphate was built from the gauche–gauche conformation of dimethylphosphate available in R.E.DD.B (see the "W-12" code).[43] For each building block a single conformation and two molecular orientations were involved in charge derivation. Second derivatives were computed to exclude the transition state structure from the charge derivation procedure. Geometry optimization, frequency calculation, and MEP computation were carried out in the gas phase using the HF/6-31G* level of theory[44] implemented in the Gaussian 2009 program (rev. A02) program,[45] whereas the charge-fitting step was performed using the RESP program (version 2.2, available at http://q4md-forcefieldtools.org/RED/resp/).[41] HF/6-31G* in MEP computation leads to implicit polarization required in condensed phase simulations when using the additive AMBER force field model.[36,41] The Connolly surface algorithm was used to compute the grid of points involved in MEP computation.[46] The molecular orientation of each optimized geometry was controlled using the rigid-body reorientation algorithm implemented in the RESP ESP charge derive (R.E.D.) program, leading to reproducible charge values.[25] Two molecular orientations based on the $N_1C_2C_3-C_3C_2N_1$, $C_3C_2O_1-O_1C_2C_3$, and $O_1C_2C_3-C_3C_2O_1$ sets of atom names for choline, ethylmethylphosphate, and 1-dodecanol (Figure 2) were involved in charge derivation, respectively. The charge-fitting step was performed using two RESP stages with hyperbolic constraint values of 0.0005 and 0.001. Intermolecular charge constraints between building block connecting groups were set to the zero value, leading to molecular fragments related to DPC and analogs. The statistics module of the RED IV program[25] and the RED Server facility[47] were used to limit errors induced by these intermolecular charge constraints. Atomic charge values are reported in Table S1 in the Supporting Information and freely available in R.E.DD.B. under the "F-92" code.

II.2. Selected Force Fields. One of the goals of this work was to validate the newly developed parameters for DPC against results obtained from MD simulations with CHARMM and GROMOS force fields and from experimental data. In particular, CHARMM36,[33] GROMOS53A6,[48] GROMOS54A7,[49,50] and GROMOS53A6/Berger[51] (often called "Berger

lipids") force fields were used in this study. The GROMOS54A7 force field is a recent update of GROMOS53A6, which introduces several improvements. Among those, a new atom type for the methyl group (i.e., CH3p) in the trimethylammonium group and new Lennard–Jones C_{12} parameters are introduced to increase the repulsion between the positively charged methyl groups and the negatively charged phosphate oxygen atoms of phosphocholine.[49] In the GROMOS53A6/Berger force field, the Lennard–Jones parameters for the methylene and methyl groups of the GROMOS53A6 force field were replaced by those parametrized by Berger. These terms are based on the united-atom version of the OPLS force field[52] and were modified to improve the agreement with the volume and heat of vaporization of pentadecane. This combination of parameters was successfully used to model phospholipids in membrane–protein simulations.[53−57] For the AMBER simulation condition, in addition to the partial charges derived as described in the previous section, bonded and nonbonded parameters were directly taken from the Amber99SB force field.[27] CHARMM and AMBER topologies were converted according to the conversion tools available within the GROMACS suite of programs.[58,59] For GROMOS simulations, the charge values for phosphatidylcholine were obtained from Chiu and co-workers.[60] The different simulations were named throughout this paper as AMBER, CHARMM, GROMOS_53A6, GROMOS_54A7, and GROMOS–Berger. Table S1 of the Supporting Information provides the list of the atom types used for DPC for the different force fields considered in this work.

II.3. MD Simulations. The GROMACS (v4.5.3) program was used in MD simulations.[58,61,62] The initial configuration of the five different simulation conditions was constructed with a "self-assembling" approach where 54 DPC monomers were placed with a random orientation (and different random seeds) in a cubic box of water with sides of 74.0 Å in length and filled with 15 176 molecules (see Table 1). This number of DPC molecules (N_{DPC}) was previously used by Tieleman et al.[18] to examine the structural and dynamic properties of preformed DPC micelles. This number was found to be in good agreement with the aggregation number experimentally determined by analytical ultracentrifugation, light scattering,[14] and ^{1}H NMR (between 44 and 61).[5,6,10] In particular, a N_{DPC} of 54 corresponds to a DPC weight of 6.5% w/w and a simulated concentration of ∼0.2 M in water. This is around 200 times higher than the experimental critical micelle concentration (cmc) of 1.1 mM[63] and not far from the concentration previously simulated.[16,18,64−68]

Table 1. Averaged Box and DPC Volumes and Simulations Lengths[a]

simulations	V^V_T	V^V_{DPC}	ρ	t_{sim}
AMBER	492 706	518.5	0.98 ± 0.01	155
CHARMM	491 867	516.7	0.98 ± 0.01	155
GROMOS_53A6	491 195	500.1	0.99 ± 0.01	170
GROMOS_54A7	493 878	526.9	0.98 ± 0.01	155
GROMOS–Berger	493 329	528.5	0.98 ± 0.01	165

[a] V^V_T and V^V_{DPC} are the Voronoi volumes in Å^3 of the simulation box and each DPC lipid, respectively. ρ values are in g/cm^3, and t_{sim} is the simulation length (in ns). Standard deviations for V^V_T and V^V_{DPC} are never greater than 1100 and 8.0 Å^3, respectively.

The TIP3P water model[69] was used in both the AMBER and the CHARMM simulations, whereas SPC[70] was involved in the GROMOS simulations. Water models were constrained using the SETTLE algorithm to keep the geometry of water rigid.[71] The initial configuration was first energy minimized with the steepest descent algorithm and an energy tolerance lower than 1000.0 kJ mol^{-1} nm^{-1}. Then, each optimized molecular system was equilibrated in the NVT ensemble at 300 K using the Berendsen thermostat[70] with a coupling constant of τ_T = 0.1 ps for 200 ps. DPC and water molecules were coupled separately to thermostatic baths as a standard rule. Subsequently, the molecular system was equilibrated at constant temperature and constant pressure (T = 300 K and P = 1.015 bar) for 300 ps using the Bussi et al. thermostat[72] with τ_T = 0.1 ps and the Parrinello–Rahman barostat[73,74] with τ_p = 3.0 ps and a compressibility of 45 × 10^{-6} bar^{-1}. During these steps, DPC molecules were harmonically restrained with a force constant of 1000 kJ mol^{-1}·nm^2 to equilibrate the solvent. Finally, the resulting molecular system was simulated in the NPT ensemble (T = 300 K and P = 1.015 bar) without any restraint using the Nosé–Hoover thermostat[75,76] and the Parrinello–Rahman barostat[73,74] with coupling constants of τ_T = 0.3 and τ_p = 1.0 ps, respectively. Periodic boundary conditions were used in MD simulations. Electrostatic interactions were treated with the particle-mesh Ewald method[77] when using the AMBER, CHARMM, and GROMOS–Berger conditions, whereas the reaction field approach[78] was used in the GROMOS_53A6 and GROMOS_54A7 simulations. Following previous studies,[58,79] a cutoff of 12 Å was used for the electrostatic and van der Waals interactions and a switching function between 10 and 12 Å was added to improve energy conservation during the CHARMM simulation. A cutoff of 10 Å was used for nonbonded interactions in the AMBER simulation. Finally, for GROMOS conditions, nonbonded interactions were evaluated with a twin-range cutoff scheme, where interactions within a shorter range cutoff (8 Å) were calculated at every step, whereas interactions were updated every 10 fs, together with the neighbor pair list with a longer cutoff (14 Å). Following ref 68 and to correct the truncation of electrostatic interactions outside the cutoff of 14 Å, a reaction field term corresponding to a relative dielectric permittivity of water of 62 was added. To integrate the MD equations of motion a 2 fs time step was used with neighbor list updates every 10 fs, whereas the P-LINCS algorithm[80] was used to restrain bond lengths to their equilibration values. Finally, the different simulations were carried out for at least 150 ns, and trajectory snapshots were collected every 2 ps. In particular, 155 ns was carried out for AMBER, CHARMM, and GROMOS_54A7, 165 ns for GROMOS–Berger, and 170 ns for GROMOS_53A6. Average properties for the DPC micelle were computed by averaging the last 55 ns of each simulation. Analysis of the trajectories was performed using the GROMACS analysis tools and homemade programs.

III. RESULTS

III.1. Aggregation Process of the DPC Micelle. We first considered the DPC aggregation process as a function of time for the different simulation conditions evaluated in this work. In Figure 3a, representative snapshots of micelle aggregation are presented for the AMBER condition. After ∼10 ns, DPC molecules aggregate to constitute large aggregates of various structures. At $t \approx 60$ ns, a micelle is formed with 53 monomers and only one DPC remains in the water phase. We estimated that between 100 and 110 ns were required to obtain a compact

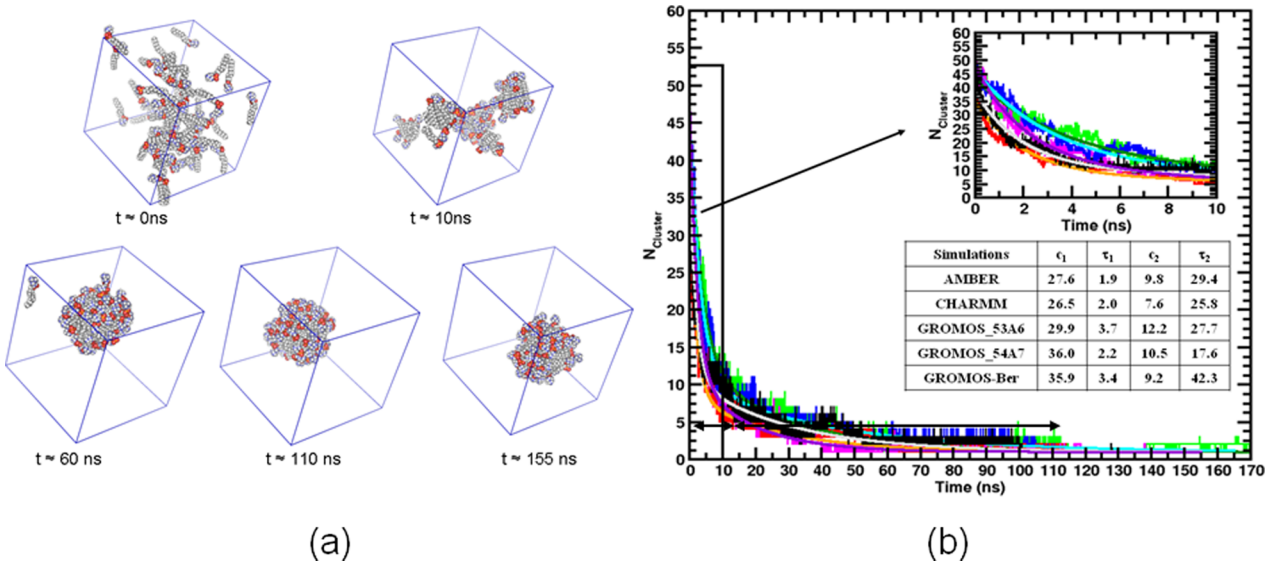

Figure 3. (a) Aggregation process of DPC monomers into a micelle vs time for the simulation performed with the Amber99SB force field. DPC lipids are drawn in the CPK style. Water is not shown for clarity. Carbons of the headgroup and alkyl tail are in light blue and gray, respectively, whereas oxygen, phosphorus, nitrogen, and hydrogen are in red, yellow, blue, and white. This figure was designed using the PyMOL program.[102] (b) Time dependence of the number of DPC clusters for the AMBER (black), CHARMM (red), GROMOS_53A6 (green), GROMOS_54A7 (magenta), and GROMOS−Berger (blue) simulations. Number of DPC clusters contained in the simulation cell were computed every 10 ps. Two horizontal arrows delimit approximately the "fast" and "slow" time scale of the micelle aggregation process. Double-exponential fitting results are shown in the inset and drawn with a continuous line in gray, orange, green, violet, and cyan for AMBER, CHARMM, GROMOS_53A6, GROMOS_53A6, and GROMOS−Berger simulations, respectively (see main text for details). τ_1 and τ_2 are in ns.

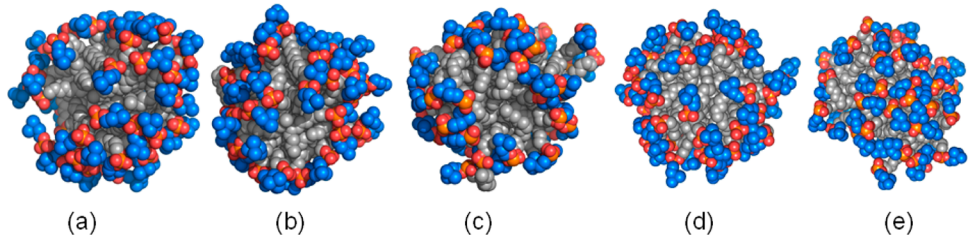

Figure 4. Final MD snapshots of the DPC micelle simulated with the Amber99SB (at $t \approx 155$ ns) (a), CHARMM36 (at $t \approx 155$ ns) (b), GROMOS53A6 (at $t \approx 170$ ns) (c), GROMOS54A7 (at $t \approx 155$ ns) (d), and GROMOS−Berger force fields (at $t \approx 165$ ns) (e). For comparison, water and hydrogen (AMBER and CHARMM simulations only) are not shown. Carbon atoms of the headgroup and alkyl tail are light blue and gray, respectively. Oxygen, Phosphorus, and Nitrogen atoms are red, yellow, and blue, respectively. This figure was designed using the PyMOL program.[102].

and stable micelle containing all 54 DPC monomers. In Figure 3b, the number of DPC clusters as function of time, $N_{cluster}(t)$ computed with the gromacs *g_clustsize* tool is reported. We considered that two DPC molecules belong to the same cluster if any of their alkyl chain carbon atoms were within 4.1 Å of each other.[81] The choice of this threshold value was validated by comparing the number of clusters determined by visual inspections of MD snapshots at different trajectory points and the number of clusters calculated using *g_clustsize*. As different random seeds were used to generate the input configuration of each molecular system, it is important to underline that the number of clusters $N_{cluster}(t = 0)$ is slightly different in the different simulations and not exactly 54 (i.e., the number of DPC monomers) but around 53. We verified that the small differences in the $N_{cluster}(t = 0)$ values between the different force fields do not significantly impact $N_{cluster}(t)$ fitting. Soon after the beginning of the production time (∼1 ns), the DPC monomers form small clusters with different aggregation kinetics depending on the simulation considered. After ∼10 ns of production, between 5 and 15 DPC clusters coexist (see the insert in Figure 3b). As previously noted,[17,23,65,82−87] the micelle aggregation process occurs with two different time scales, one "fast" (time t_{fast} < 10 ns) and one "slow" (time t_{slow} between 10 and ∼110 ns) decay process (see the insert in Figure 3b). The "fast" process is generally associated with a quick aggregation of DPC monomers into small clusters and a fusion/fragmentation of these small clusters into larger ones.[88] During the slow process, the different aggregates merge to form a single and stable micelle. To characterize these time scales, the $\Delta N_{cluster}(t) = N_{cluster}(t) - N_{cluster}(t_\infty)$ function was fitted by a double-exponential function to the relation $c_1 e^{-t/\tau_2} + c_2 e^{-t/\tau_2}$ where $N_{cluster}(t_\infty) = 1$. Here, τ_1 and τ_2 are the characteristic relaxation times for the fast and slow processes, respectively.[88,89] In this model c_1 and c_2 represent the waning number of the number of clusters involved in the two simulation periods previously defined. Figure 3b provides the fitted parameters obtained from the $N_{cluster}(t)$ function for each simulation condition. As demonstrated by these values, the kinetics of the micellization process slightly differs between the force fields. In particular, we observed that in the AMBER and

CHARMM simulations, the DPC monomers aggregate with a similar kinetic (with $\tau_1 \approx 2.0$ ns and $\tau_2 \approx 25.8-29.4$ ns). In case of the GROMOS54A7 simulation, the fast aggregation process is similar to CHARMM and AMBER simulations ($\tau_1 \approx 2.2$ ns) but is 1.6 times faster than in the GROMOS_53A6 and GROMOS_Berger simulations (τ_1 = 3.4−3.7 ns). The slow process in GROMOS54A7 is also found to be faster than in all other simulations, with τ_2 = 17.6 ns. It is difficult to rationalize these results because different water models and simulation conditions were used in this study, and these parameters should impact water-mediated interactions. We wish also to point out that the micelle aggregation processes occur more slowly in this study than, for example, in ref 17, where the DPC aggregation process was at least 5 times faster. These differences might be related to differences in the simulation methods employed to take into account the nonbonded interactions or control the system temperature (Dr. S. J. Marrink, personal communication, Feb 2012). Finally, Figure 4 presents the final snapshot of the DPC micelle obtained at the end of each simulation.

III.2. Volumetric Properties of the Micelle. In this section, we focus on the micelle volumetric properties measured after self-aggregation. For this purpose, a GROMACS-compatible computational tool, *trjVoronoi*,[90] was developed. This program uses some of the voro++ classes and libraries, developed by C. H. Rycroft,[91] to compute at each simulation time frame the Voronoi volume (V^V) of each atom of the system. Voronoi−Delauney tessellation[92] defines a unique volume for each atom or molecule as a function of their positions. Given that the sum of the V^V of all atoms of the simulation box is equal to the volume of the simulation box itself, we verified that the relative difference between the volume computed from the simulation box size and the volume obtained from the sum of all atomic V^V was negligible (here, within the numerical error). Explicit hydrogen atoms were not included in the Voronoi volume computation as performed in previous studies.[93,94] Excluding explicit hydrogen atoms from the Voronoi calculation has the advantage of reducing by a factor of 2 the CPU time required to compute this volume at each frame with a relative error with respect to the all hydrogen calculation lower than 1.0%. The computed average Voronoi volumes for each molecular system V^V_T and each DPC molecule V^V_{DPC} are reported in Table 1. Our results show that the V^V_T values for the different simulations are close to each other (between 491 195 and 493 878 ± 1100 Å^3). In the case of the DPC Voronoi volume, more noticeable differences are observed between the "all-atom" and the "united-carbon atom" force fields. Indeed, the V^V_{DPC} values obtained from the CHARMM and AMBER simulations are equal, on average, 517.6 ± 1.3 Å^3, lower than the values found for the GROMOS_54A7 and GROMOS−Berger simulations (527.7 ± 1.3 Å^3). In the case of the V^V_{DPC} value obtained from GROMOS_53A6 simulations (500.1 ± 3.0 Å^3), this value is found significantly different than the others. These differences may be related to the different methods used to evaluate the electrostatic interactions in the GROMOS conditions (i.e., reaction field versus PME) and/or by adjustment of the Lennard−Jones parameters for the methylene and methyl groups in the GROMOS_54A7 and GROMOS−Berger force fields as indicated in section II.2. Finally, the V^V_{DPC} values obtained in the different simulations are not far from the apparent volume obtained by the ultracentrifugation experiment (476.2 Å^3) at 295 K[14] or deduced from the DPC density (548.1 Å^3).[4,15]

III.3. Size and Shape of the Micelle. Here, we report on results about the size and shape of the DPC micelle in the different simulation conditions considered in this work. A characteristic feature related to the micelle size is the radius of gyration, R_g, of the micelle. The instantaneous value of R_g over the course of the different simulations is described in Figure 5.

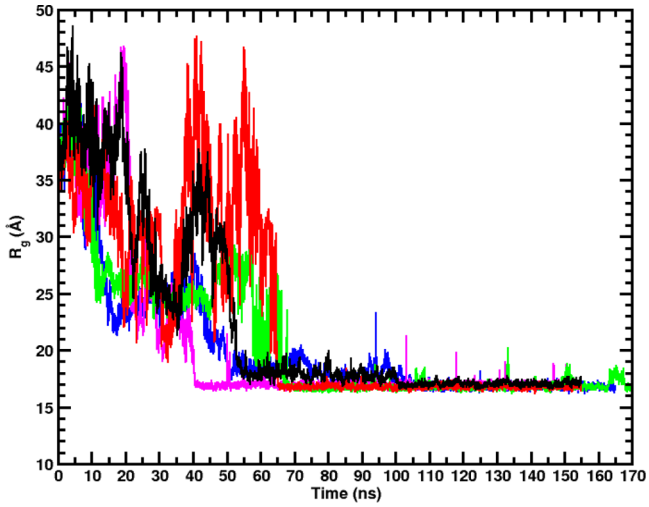

Figure 5. Radius of gyration as a function of time for the AMBER (black), CHARMM (red), GROMOS_53A6 (green), GROMOS_54A7 (magenta), and GROMOS−Berger (blue) simulations.

We notice that R_g values reach a stable value around 17 Å after 100−110 ns depending on the force field considered. By opposition to the number of clusters $N_{cluster}$, R_g values display large oscillations just before settling to the 17 Å value, demonstrating that formation of the final cluster occurs rather abruptly within 2−3 ns. The R_g mean value obtained over the last 55 ns of each simulation is in the range of 16.8−17.1 Å ± 0.1 Å as shown in Table 2 for the different simulations. This range of values agrees well with those reported by Lazaridis et al.[23] for micelles with a N_{DPC} value between 49 and 63 simulated with the CHARMM27 force field. This 17 Å value is also slightly lower than the R_g value obtained in ref 18 (17.4 Å) for a micelle composed of 60 DPC molecules modeled with the CHARMM22 force field. From the expression $R_M = R_g(5/3)^{1/2}$ is deduced the mean effective radius, R_M, for a micelle represented as a solid sphere of uniform density.[95] The R_M value can be compared to the micelle radius obtained in experiments and to the value obtained from the distance between the micelle center of mass (COM) and the density maximum of the micelle choline groups (see section III.4). We calculated R_M values of 21.9, 21.7, 21.8, 22.1, and 21.7 Å for AMBER, CHARMM, GROMOS_54A7, GROMOS_53A6, and GROMOS−Berger, respectively. As a rather large uncertainty exists for the experimental aggregation number (experimental N_{DPC} oscillates between 44 and 61),[5,6,14] it is difficult to obtain a single value for the experimental micelle size. For example, Kallick et al.,[5] Gao and Wong,[6] and Göbl et al.[10] determined a hydrodynamic radius between 18.6 and 23.3 Å from NMR self-diffusion experiments for micelle composed of 44−61 DPC molecules.

The micelle shape was also investigated by computing the principal moments of inertia (MOI), I_1, I_2, and I_3 ($I_1 > I_2 > I_3$) from the inertia tensor. The micelle asymmetry parameter α defined as $\alpha = (2I_1 - I_2 - I_3)/(I_1 + I_2 + I_3))$ was also

Table 2. Average Dimensions and Shape of the Micelle[a]

micelle	R_g	I_1	I_2	I_3	I_1/I_3	I_1/I_2	I_2/I_3	α
AMBER	17.0	4.04 ± 0.18	3.72 ± 0.14	3.25 ± 0.14	1.24	1.08	1.14	0.10 ± 0.03
CHARMM	16.8	3.88 ± 0.15	3.57 ± 0.12	3.21 ± 0.14	1.20	1.09	1.11	0.09 ± 0.03
GROMOS_53A6	16.9	4.04 ± 0.15	3.68 ± 0.25	3.11 ± 0.17	1.29	1.09	1.20	0.12 ± 0.05
GROMOS_54A7	17.1	3.97 ± 0.18	3.62 ± 0.16	3.23 ± 0.13	1.23	1.10	1.12	0.11 ± 0.02
GROMOS−Berger	16.8	3.92 ± 0.17	3.60 ± 0.14	3.15 ± 0.12	1.24	1.09	1.14	0.10 ± 0.03

[a]Radii of gyration, moments of inertia I_1, I_2, and I_3 (in 10^4 amu.nm^2), and the asymmetry parameter α $(2I_1 - I_2 - I_3)/(I_1 + I_2 + I_3))$ were computed from the last 55 ns of each simulation. Statistical error (maximum error) for R_g is always lower than 0.1 Å.

computed.[18] An α value lower than the 0.05 threshold corresponds to a spherical aggregate. Table 2 reports the values of these parameters averaged over the last 55 ns of simulations. The mean values of I_1, I_2, and I_3 for the different simulation conditions are 3.97 ± 0.07, 3.64 ± 0.06, and 3.19 ± 0.22 10^4 amu.nm^2 and 12.35%, 8.35%, and 3.25% higher than the values obtained by Tieleman et al.[18] In this study, the mean MOI ratios are I_1/I_3 = 1.24 ± 0.39, I_1/I_2 = 1.09 ± 0.1, and I_2/I_3 = 1.14 ± 0.11, whereas the α value is in the range of 0.09−0.12 ± 0.03, which is not far to 0.05, as previously reported in ref 18. These parameters confirm that the DPC micelles computed in the different simulation conditions are slightly ellipsoidal and have a prolate-like geometry. This is in agreement with a previous MD investigation[16] and experiments.[14,15]

III.4. Density Profiles of the Micelle. The mean radial mass density profiles $\rho(r)$ were computed for the relevant chemical groups of the micelle as a function of the distance, r, from the micelle center of mass (COM) to compare the spatial localization of these chemical groups. Here, we focused on the whole DPC headgroup, the phosphate, the choline groups, the dodecane tail, and water. The $\rho(r)$ functions, presented in Figure 6, were computed every 2 ps and averaged over the last 55 ns for each simulation. This figure clearly shows that the different simulations display similar density profiles for the different chemical groups considered. More specifically, we found that in the different simulations the micelle oil core $\rho(r)$ profile for the DPC alkyl chain extends from 0 to ∼16.0 Å with a mean density of 0.78 g·cm^{-3}, close to the dodecane bulk density (0.745 g·cm^{-3}).[96,97] On the other hand, the mean alkyl $\rho(r)$ profile obtained from the GROMOS_53A6 and GROMOS−Berger simulations slightly differ with these of AMBER, CHARMM, and GROMOS_54A7. This observation might be related to differences in the aliphatic chain packing and conformation of the micelle oil core observed for these two models (see section III.6). In the different simulation conditions, the phosphatidylcholine headgroup has a thickness within 8.0−9.0 ± 1.0 Å and extends from ∼14 to 23 Å of the micelle COM with a strong peak at 18.7 Å (see the insert in Figure 5). The average thickness value of the DPC headgroup (9.8 ± 0.3 Å) computed by subtracting the semiaxis lengths of the hydrophobic core, a_{HC}, b_{HC}, and c_{HC}, from those of the whole micelle, a_M, b_M, and c_M (see Table S3 in the Supporting Information), is consistent with values obtained in previous DPC simulations.[16,18] Neutron reflectivity experiments have shown that the phosphatidylcholine headgroup has a thickness of 10−11.5 ± 2.0 and 8.0 ± 1.5 Å at the air−water interface and in bilayer, respectively.[98−101] We also calculated with the PyMol program[102] that the phosphocholine headgroup has a length of ∼10.0 Å in the extended conformation (i.e., "all dihedral angle trans"). These results indicate that the DPC headgroup adopts a bent conformation in the micelle, which is favored by the gauche−gauche conformations for the phosphodiester dihedral angles (i.e., $C_6O_7P_8O_{11}$ and $O_7P_8O_{11}C_{12}$, see Figure 1). The negatively charged phosphate group is in close contact with the positively charged trimethylammonium (see section III.6).[103] We also found that the position of the peak of the choline group slightly varies with the considered force field, whereas that of the phosphate peak remains nearly constant (at 18.3 Å from the micelle COM). For the AMBER and CHARMM simulations, the choline peak is located at around 19.0 Å from the micelle COM (not far from the R_M values discussed in section III.3), whereas in the GROMOS simulations the peak is shifted 1.5 Å toward the micelle COM. Finally, the overlap between the water and the DPC alkyl tail densities observed for the different simulations indicates that water molecules interact with atoms of the alkyl chain located at the micelle surface and solvate the DPC headgroup at different degrees depending on the simulation conditions (see the next section).

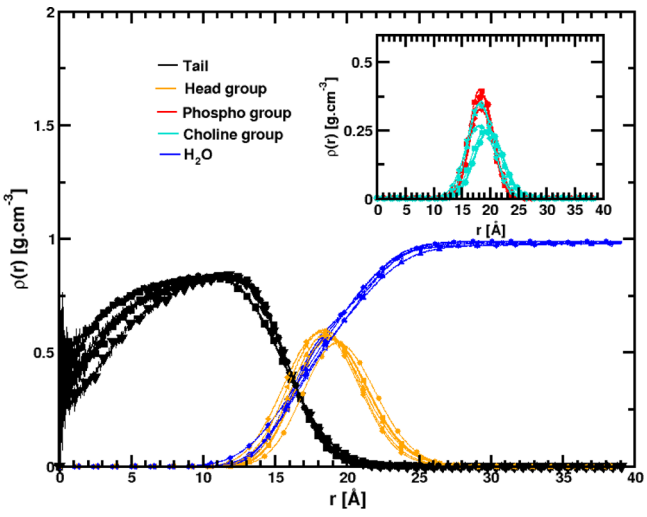

Figure 6. Average radial density profiles $\rho(r)$ with respect to the center of mass (r = 0 Å) of the DPC micelle for the AMBER (●), CHARMM (■), GROMOS_53A6 (♦), GROMOS_54A7 (▲), and GROMOS−Berger (▼) simulations. (Inset) Average $\rho(r)$ of the micelle hydrophobic core (black), phosphatidylcholine headgroup (orange), and water (blue).

III.5. Micelle Hydration Properties. Turning our attention to DPC−water interactions, contacts between water molecules and the DPC micelle were investigated by computing the solvent-accessible surface area (SASA) using two different methods. In the first approach, the double cubic lattice method[104] as implemented in the GROMACS *g_sas* tool was used to compute the Connolly surface. In the second approach, the Voronoi surface was obtained using the newly developed *trjVoronoi* program described above. Voronoi areas were computed by summing up the surfaces of the Voronoi polyhedral facets shared between the atoms of DPC and

dx.doi.org/10.1021/ct3003207 | J. Chem. Theory Comput. 2012, 8, 4610−4623

water. As for the Voronoi volume calculation described in section III.2, explicit hydrogen atoms were not involved in the surface calculations and the relative differences between the surface area fractions computed with and without the hydrogen atoms were found negligible (i.e., lower than 1.0%). Concerning the Connolly surface calculations and for the sake of consistency, we used a probe with a radius of 1.4 Å for water and the atomic van der Waals radii defined by Tsai et al.[105] Surface calculations were carried out for MD snapshots selected every 10 ps over the last 55 ns of simulations. The mean Connolly and Voronoi areas computed for the DPC molecule and the DPC headgroup, $SASA_{total}$ and $SASA_{head}$, respectively, are reported in Table 3. In addition to these values, the mean surface fraction shared between the water and the DPC alkyl chain, i.e., $f_{tail} = 1 - (SASA_{head}/SASA_{total})$, computed using the two methods is also reported in Table 3.

Table 3. Average Water−DPC Surface Contact Per Molecule[a]

micelle	$SASA_{total}$	$SASA_{head}$	f_{tail}
AMBER	(225.8) 223.9	(154.9) 173.9	(31.3) 22.3
CHARMM	(214.8) 217.7	(160.4) 173.7	(25.3) 20.2
GROMOS_53A6	(200.6) 193.7	(136.4) 145.7	(32.0) 24.7
GROMOS_54A7	(228.2) 223.7	(160.2) 177.8	(29.8) 20.5
GROMOS−Berger	(207.6) 209.9	(155.6) 169.5	(25.4) 19.9

[a] $SASA_{total}$ and $SASA_{head}$ (in Å^2) are the average water surface area of the DPC molecule and its head group, respectively. f_{tail} (in %) is the average surface fraction shared between the water and the DPC alkyl chain. SASA values (in Å^2) in parentheses are obtained with the *trjVoronoi* program,[90] while the others from the Connolly surface and the GROMACS *g_sas* tool. Statistical errors (maximum errors) are always lower than 3.0% for the surfaces. Values were computed from the last 55 ns of each simulation.

We first notice that the SASA converged to a stable value independently of the simulation conditions and remained constant until the simulation ended. At shorter times, the dynamics of the instantaneous values of the SASA (Figure S1 in the Supporting Information) showed slow and fast decay time scales, which are evocative of the behavior of the aggregation number discussed in section III.1. Concerning the SASA values for the whole detergent and its headgroup, the Voronoi and Connolly methods led to similar results and differences lower than 8% in the computed surfaces were observed. Consistent with previous work,[106] the GROMOS_53A6 force field leads to smaller SASA values and underestimates the surface area of the phosphatidylcholine headgroup. This limitation was corrected in the GROMOS−Berger and GROMOS_54A7 force fields by modifying the van der Waals parameters of the methyl group in the trimethylammonium group. In this work, the surface fraction, f_{tail}, obtained from Voronoi and Connolly is in the range of 25.4−32.0% and 19.9−24.7%, respectively. These values confirm the results reported in Figure 6 for the DPC headgroup hydration and demonstrate that the micelle hydrophobic core is well protected from the solvent. A pictorial view of the exposed hydrophobic surfaces is shown in Figure 4.

To further investigate the DPC headgroup hydration, the mean radial density functions, $g_{(X-OW)}$, between the water oxygen, O_w, and six DPC atoms (namely, nitrogen (X = N), phosphorus (X = P), and oxygen atoms belonging to the phosphate (X = O_9 and O_{10}) and ester (X = O_7 and O_{11}) groups (see Figure 7a−d)) were computed. Table 4 presents the mean number of water molecules in the first hydration shell of these atoms obtained by integrating the corresponding $g_{(X-OW)}$ functions until their first minimum after the first peak. We notice that the trimethylammonium group has about 18.0 water molecules in its first hydration shell for the different simulation conditions except for GROMOS_53A6, for which a value of 15.3 is found. The interaction between trimethylam-

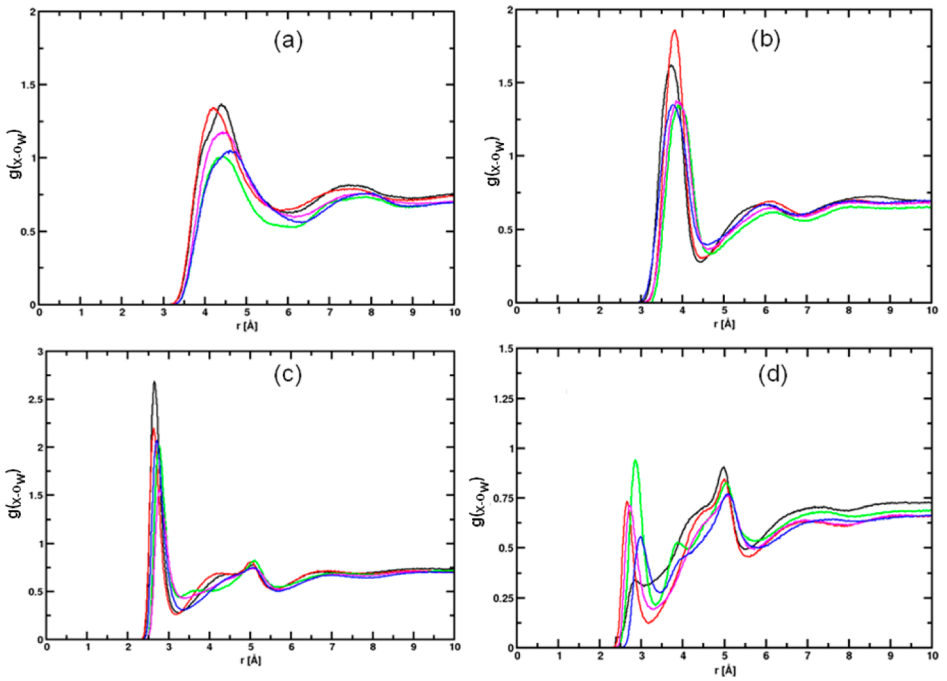

Figure 7. Average radial density functions $g_{(X-OW)}$ between nitrogen (X = N) (a), phosphorus (X = P) (b), phosphate oxygen atoms (X = O_{9-10}) (c), and phosphoester oxygen atoms (X = O_{7-11}) (d) atoms of the DPC headgroup with water oxygen (O_w) (see Figure 1) for the AMBER (black), CHARMM (red line), GROMOS_53A6 (green), GROMOS_54A7 (magenta), and GROMOS−Berger (blue).

Table 4. Average Micelle Hydratation Properties[a]

n_{X-OW}	AMBER	CHARMM	GROMOS_53A6	GROMOS_54A7	GROMOS−Berger
N	18.6	18.4	15.3	17.2	18.7
P	6.4	6.6	7.3	6.6	6.4
O_{9-10}	2.4	2.3	2.4	2.1	2.7
O_{7-11}	0.3	0.8	1.3	1.0	1.1
O_7	0.3	0.8	0.5	0.9	0.9
O_9	2.7	2.3	3.2	2.1	2.8
O_{10}	2.7	2.3	1.7	2.1	2.2
O_{11}	0.6	0.8	0.9	1.1	0.9

[a]Average numbers of water in the first hydration shell, n_{X-OW}, for headgroup nitrogen (X = N), phosphorus (X = P), and oxygen atoms (X = O_7, O_9, O_{10}, and O_{11}). Values have been obtained by integrating the pair correlation functions $g_{(X-OW)}$ up its first minimum at 5.9, ∼4.5, and 3.3 Å for the nitrogen, phosphate, and ester oxygen atoms, respectively.

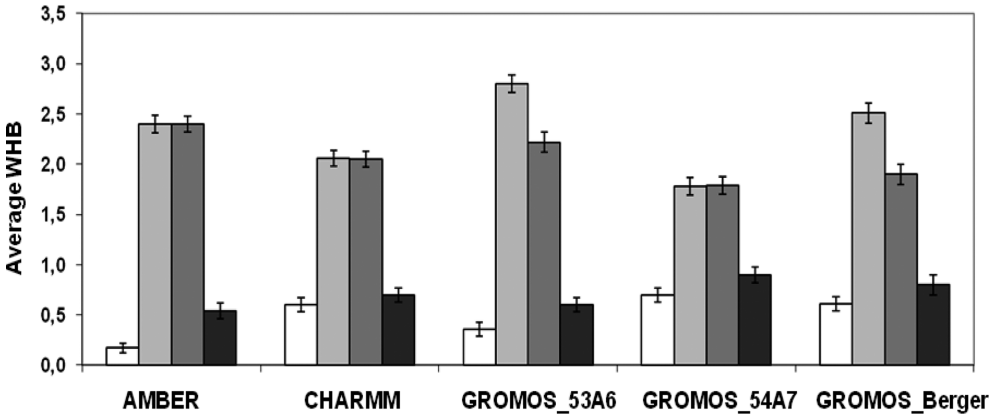

Figure 8. Distributions of the average number of water hydrogen bonds for each DPC oxygen atom (O_7, O_9, O_{10}, and O_{11} in white, gray, dark gray, and black, respectively).

monium and water molecules is characterized by a first broad peak at a distance of around 4.5 Å compared to the other $g_{(X-OW)}$ values, in agreement with previous publications.[107,108] This indicates that the nitrogen atom in trimethylammonium is shielded from the solvent by methyl groups. For the phosphorus atom, we observed n_{P-OW} values around 6.5 for the different simulation conditions except for GROMOS_53A6 for which n_{P-OW} is 11.0% larger. The n_{N-OW} and n_{P-OW} values in the AMBER, CHARMM, GROMOS54A7, and GROMOS−Berger simulations are consistent with the values obtained by Wymore et al.[16] for a micelle of 60 DPC molecules simulated with the CHARMM22 force field (n_{N-OW} = 21.3 and n_{P-OW} = 8.0, respectively). For the sake of comparison, these values are lower than those reported by Foglia et al.[107] for a phosphatidylcholine headgroup in water (n_{N-OW} = 23.0 and n_{P-OW} = 8.0) and higher than those obtained in refs 108−111 for membrane-forming phospholipids (n_{N-OW} < 16.0 and n_{P-OW} = 6.0). The O_9 and O_{10} phosphate oxygen atoms have a similar hydration with, on average, 2.6 ± 0.4 and 2.2 ± 0.4 water molecules in their first shells. In contrast to the phosphate oxygen atoms, the two O_7 and O_{11} ester oxygen atoms are less solvated with, on average, 0.7 ± 0.3 and 0.9 ± 0.2 water molecules in their first shells, respectively. This indicates that these atoms are partially shielded from the solvent by the size of the choline group and/or the alkyl chain. These values are comparable to those obtained previously in experiments (∼0.6)[107] or in simulations (∼0.4).[108−111] We pointed out that the significantly lower hydration of the O_7 and O_{11} oxygen atoms (0.3 and 0.6, respectively) in the AMBER simulation are probably related to different conformations of the choline−phosphate and phosphate−alkyl chain junctions of the headgroup compared to the other force fields that may affect the accessibility of the these atoms to water. The existence of two peaks at ∼2.8 and ∼5.0 Å in the radial density function in the ester oxygen−water functions, $g_{(O7-9-OW)}$ (Figure 7d), indicates two well-defined hydration shells. The first peak indicates the existence of hydrogen bonds between water and the oxygen ester atoms, whereas the second peak, at a longer distance, reflects the presence of a water molecule that forms two hydrogen bonds between the ester and the phosphate oxygen atoms.[107,108]

Hydrogen bonds formed between the phosphatidylcholine oxygen atoms and water (WHB) were also investigated during the last 55 ns of each simulation. We considered a WHB if the O_X-O_W distance was lower than 3.25 Å (i.e., the $g_{(OX-OW)}$ first minimum) and the $O_w-H_w\cdots O_x$ angle is greater than 145°.[110,111] In Figure 8 a histogram about the average number of WHB for the different headgroup oxygen atoms is presented. As shown in this figure, the corresponding WHB values vary with the force fields: GROMOS53A6 has the largest number of WHB and then follows GROMOS−Berger, AMBER, CHARMM, and GROMOS54A7. These results are in agreement with the variations of the n_{P-OW} and n_{ox-OW} values reported in the previous paragraph. On average, each DPC headgroup forms a total of 5.2−6.0 WHB. As expected, the phosphate oxygen atoms are found to form more WHB (1.8−2.4 ± 0.1) than the ester oxygen atoms (0.7−0.9 ± 0.1). This is a consequence of the poor hydration of the latter compared to the former. The lower number of WHB for the O_7 atom in the AMBER simulation compared to other simulations is a

dx.doi.org/10.1021/ct3003207 | J. Chem. Theory Comput. 2012, 8, 4610−4623

consequence of the poor hydration of this atom noted in the previous paragraph. The WHB values for the O_7 and O_{11} atoms are found to be slightly lower in this study than the values obtained for a phosphatidylcholine headgroup in water (0.8)[107] and larger than those found for phospholipid bilayer (0.1 and 0.3, respectively).[110,111] Finally, we observed that water molecules form hydrogen bonds between the ester and the phosphate oxygen atoms belonging to adjacent DPC head groups in all simulations, as illustrated in Figure 9 for the AMBER condition. Formation of water bridges between phospholipids was also revealed in previous membrane MD simulation studies.[108,111]

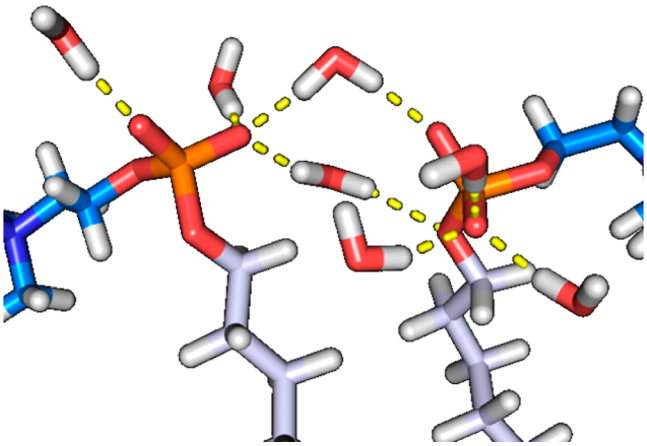

Figure 9. Representative snapshots for the water−lipid and lipid−water−lipid hydrogen-bond network (yellow dashed lines) for two selected DPC molecules extracted from the AMBER simulations (see main text for details). This figure was created using the PyMOL program.[102]

III.6. Conformational Properties of DPC. To account for the differences in the headgroup hydration of the micelle in the different simulation conditions, the conformation of DPC molecules was examined through characteristic headgroup and alkyl tail dihedral angles. For this purpose, we computed the mean normalized dihedral angle distributions P(Φ) for the last 55 ns of each simulation and calculated the percentage of trans conformation, p_{trans} (defined as $-60° < \Phi < +60°$), for each dihedral angle. First, we characterized the DPC phosphatidylcholine headgroup conformation by examining the $N_4C_5C_6O_7$, $C_5C_6O_7P_8$, $C_6O_7P_8O_{11}$, $O_7P_8O_{11}C_{12}$, and $P_8O_{11}C_{12}C_{13}$ dihedral angles.[112−114] The mean relative trans populations, p_{trans}, extracted from P(Φ) are presented in Table 5. The $N_4C_5C_6O_7$ dihedral angle was found to be mostly in the gauche state in all simulations. The corresponding p_{trans} value is higher (∼17.8%) in the AMBER than in the CHARMM and GROMOS simulations (5.7% and 3.0−3.7%, respectively). The gauche population for the $N_4C_5C_6O_7$ dihedral angle is consistent with results obtained for the phosphocholine headgroup of 1,2-dimyristoyl-*sn*-glycero-3-phosphocholine (DMPC), 1,2-dipalmitoyl-*sn*-glycero-3-phospcholine (DPPC) phospholipids obtained in previous MD simulations,[16,114] DFT calculations,[113] or ^1H and ^{13}C NMR experiments.[112,115] The gauche conformation of the $N_4C_5C_6O_7$ dihedral is favored by charges of opposite sign in the trimethylammonium and phosphate groups.[112] Independently of the force field considered, the dihedral angles involving the ester oxygen atoms connecting the choline ($C_5C_6O_7P_8$) and the phosphate ($C_6O_7P_8O_{11}$) groups adopted trans and gauche conformations with p_{trans} values in the range of 65.0−83.6% and 7.0−20.0%, respectively. These results are consistent with previous observations.[16,112−115] Finally, the $O_7P_8O_{11}C_{12}$ and $P_8O_{11}C_{12}C_{13}$ dihedral angles in the five simulations were also found in gauche conformations (3.3−18.0% and 12.0−47.7%, respectively) with variations depending on the different simulation conditions.

The conformation and flexibility characteristics of the DPC alkyl chain were analyzed by computing the average fraction of trans and the mean gauche ↔ trans transition time for the $O_{11}C_{12}C_{13}C_{14}$ dihedral angle and the nine alkyl Csp^3−Csp^3−Csp^3−Csp^3 dihedral angles (i.e., $C_{12}C_{13}C_{14}C_{15}$−$C_{20}C_{21}C_{22}C_{23}$). As in ref 18, we used a well width of 60° and a transition is counted if a dihedral changes from one potential well to another. It is well known that the alkyl chain in the micelle core has similar characteristics to liquid alkane.[51,116−118] Consequently, the results about the DPC alkyl chain conformation were compared to these obtained from simulations of liquid *n*-tridecane carried out with the Amber99SB, CHARMM36, GROMOS54A7, and GROMOS_Berger parameters at $T = 300$ K and $P = 1.015$ bar (see Supporting Information). We choose *n*-tridecane because this alkane has an equivalent number of methylene groups to the DPC alkyl chain. The results obtained for the DPC alkyl chain are summarized in the last two rows of the Table 5 and in Figure 10, whereas results for liquid *n*-tridecane are reported in Figures S2 and S3 and in Table S4 of the Supporting Information. Figure 10 and Table 5 show that in the DPC micelles the first and last dihedral angles of the DPC alkyl chain (i.e., $O_{11}C_{12}C_{13}C_{14}$ and $C_{20}C_{21}C_{22}C_{23}$) are substantially in a gauche state like the first and last CCCC angles (i.e., $C_1C_2C_3C_4$ and $C_{10}C_{11}C_{12}C_{13}$) of *n*-tridecane (see Figure S3a, Supporting Information). These results are consistent with those obtained in micelles with a *n*-dodecane tail.[16,18,28,34,119−122] We also observed that the p_{trans} values for $O_{11}C_{12}C_{13}C_{14}$ are similar (65.0−70.0%) in the AMBER,

Table 5. Average Trans Populations for Selected DPC Dihedral Angles[a]

p_{trans}	AMBER	CHARMM	GROMOS_53A6	GROMOS_54A7	GROMOS−Berger
$N_4C_5C_6O_7$	17.8	5.7	3.0	3.0	3.7
$C_5C_6O_7P_8$	83.6	70.4	68.0	65.0	75.9
$C_6O_7P_8O_{11}$	9.0	13.2	7.0	20.0	14.0
$O_7P_8O_{11}C_{12}$	6.0	13.5	10.0	18.0	3.3
$P_8O_{11}C_{12}C_{13}$	12.0	47.7	30.0	31.0	15.0
$O_{11}C_{12}C_{13}C_{14}$	70.0	64.0	53.0	67.0	55.0
CCCC	84.3	70.7	60.1	71.5	59.8

[a] p_{trans} is the relative trans population (i.e., defined as $-60° < \Phi < +60°$) for the examined dihedral angle (in %). Statistical errors (maximum errors) are always lower than 0.3% (see the main text for details).

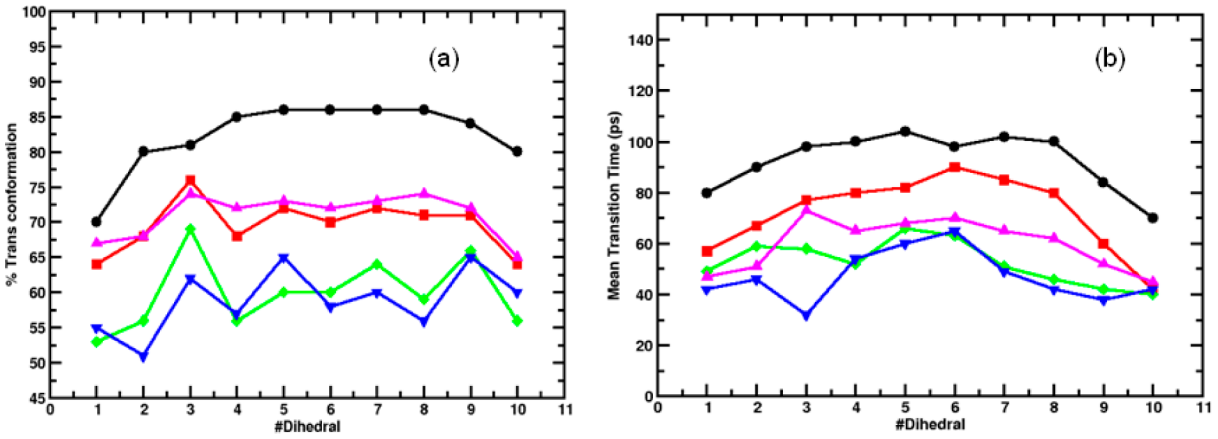

Figure 10. Average relative trans population (a) and mean trans ↔ gauche transition time (b) for CCCC angles along the DPC alkyl chain for the AMBER (black, ●), CHARMM (red, ■), GROMOS_53A6 (green, ♦), GROMOS_54A7 (magenta, ▲), and GROMOS−Berger (blue, ▼) simulations. Error in the mean transition time value is less than 10%. Note that the first dihedral is $O_{11}C_{12}C_{13}C_{14}$ and last $C_{20}C_{21}C_{22}C_{23}$.

CHARMM, and GROMOS54A7 simulations and are ∼10−15% higher than p_{trans}'s obtained in the GROMOS53A6 and GROMOS_Berger simulations (p_{trans} = 50.0−55.0%). Concerning the last dihedral of the chain, $C_{20}C_{21}C_{22}C_{23}$, the p_{trans} values of the CHARMM and the three GROMOS's simulations are between 55.0% and 65.0%, whereas AMBER produces slightly higher values. Concerning the carbon atoms in the middle of the DPC alkyl chain, p_{trans} values reach a plateau in all simulation conditions. Specifically, p_{trans} is found between 67.0% and 72.5% in the CHARMM36 and GROMOS 54A7 simulations similar to results in *n*-tridecane (p_{trans} = 70.0−75.0%). We also obtained in GROMOS53A6 and GROMOS_-Berger simulations p_{trans} values of 55.0% and 67.5%, indicating that in these conditions the DPC alkyl chain displays more "disordered" conformations compared to CHARMM and GROMOS 54A7 micelles. For carbon atoms in the center of the DPC alkyl chain in the AMBER simulation, p_{trans} values are within 80.0−87.0% in the AMBER simulation, similar to results calculated for *n*-tridecane (see Figure S3a, Supporting Information), indicating that the DPC alkyl chain displays a more ordered conformation that in the other simulation conditions.

Klauda et al. compared the conformational energy barriers for different short linear (*n*-butane to *n*-heptane) and longer (*n*-decane to *n*-pentadecane) alkanes modeled with the AMBER and CHARMM27(r) force fields.[117] These authors reported that the alkyl CCCC dihedral angle displays a slightly higher trans/gauche barrier of 0.7 kcal/mol for AMBER compared to CHARMM. This leads in AMBER to a small overestimation for the trans population compared to CHARMM (p_{trans} ≈ 71.0%) and experiment (p_{trans} ≈ 68.0%).[116] However, experimental equilibrium properties such as density or isothermal compressibility are correctly reproduced, Figures 10b and Figure S3b, Supporting Information, show the mean gauche ↔ trans transition time for the alkyl chain in the DPC micelle and for liquid *n*-tridecane, respectively. In all simulations, the dihedral transition times of the first and last dihedral angles of the alkyl chain are comparatively shorter than for the other dihedral angles. Also, comparison of Figures 10b and S3b, Supporting Information, shows that the transition times obtained in the micelle are usually higher than those obtained in liquid *n*-tridecane. This observation confirms previous results obtained by Tieleman et al.[18] and Bogusz et al.[120] in octylglyosides and DPC micelles where alkyl dihedral angle transitions in micelles are slower that those in liquid alkanes. Specifically, in the CHARMM and GROMOS conditions, transition times for the first dihedral are around 40−60 ps, whereas a plateau of 60−80 ps is reached for central dihedral angles followed by a drop to 40 ps for the last dihedral angle. Similar to our results for p_{trans}, the AMBER transition times are consistently ∼20% higher than those obtained from the other force fields. Thus, our simulation results indicate that the alkane chain is slightly more rigid with the AMBER force field that with the other potentials considered here.

IV. CONCLUSION

In this paper we presented the first comparative MD investigation for a DPC micelle performed in condensed phase using current force fields available in academics MD simulation packages and results about the derivation and the validation of a new set of RESP charges for the DPC surfactant to be used in MD simulations with the Amber99SB force field. Atomic charge derivation for the DPC molecule was performed using the "building block" approach, and the procedure followed ensures reproducible RESP charge values. We validated this approach by performing MD simulations on a DPC micelle using a "self-assembling" protocol, where 54 DPC monomers were randomly placed in the simulation box as the initial condition of each simulation. Although Amber99SB was originally designed for protein simulations, MD results obtained with our new potential are found to reproduce reasonably well important structural properties (such as size, shape, interior of the DPC micelle) compared to the other force fields as well as experimental data. In the case of other properties such as the headgroup and alkyl chain conformations or the micelle hydration, results obtained with Amber99SB show some differences from the other force fields: the trans population of the dihedral angles of the DPC alkyl chain modeled with Amber99SB is slightly over stabilized.

Our self-assembling approach shows that the micelle aggregation process occurs in two time scale characterized by fast and slow time scales. Consistent with previous simulations[18,23] and experiments,[6,10] the mean radius of gyration and the effective radius of the micelle are near 17 and 22 Å, respectively. Also in agreement with previous results,[14−16] the DPC micelle in AMBER simulation conditions is slightly ellipsoidal with a prolate-like geometry. Overall, the

radial density profiles show that water penetrates into the micelle and interacts with the micelle hydrophobic core. The $SASA_{head}$ values of DPC with the Amber99SB and CHARMM36 force fields are similar and represent 70−80% of the total micelle surface in contact with water. In the case of GROMOS simulations, consistent with previous observations,[106] we confirm that GROMOS53A6 significantly underestimates the SASA value of the DPC headgroup. Indeed, adjustments of the methyl Lennard−Jones parameters in GROMOS54A7 and GROMOS−Berger parameter lead to more reliable SASA values, which is in agreement with the values obtained from the AMBER and CHARMM simulations. Consistent with previous simulations[6,109,114] and experimental results,[107,123] the trimethylammonium and phosphate groups display similar hydration values independent of the force field considered with ∼18 and ∼7 water molecules in the first shell. In general, the ester oxygen atoms bonded to the choline group and the alkyl tail are less solvated than the phosphate oxygen atoms, in agreement with previous simulations.[16,111] Investigating the hydrogen-bond formation between water molecules and ester and phosphate oxygen lead to results where water molecules form, on average, 5.2−6.0 hydrogen bonds per headgroup and the number of WHB depends on the oxygen atom itself in the headgroup. We also notice that water can form sporadic hydrogen-bond bridges between oxygen atoms of two adjacent DPC head groups as previously described for phospholipid bilayers.[108,111]

The reported AMBER force field for DPC is consistent with the Amber99SB force field and reproduces reasonably well DPC micelle properties. We think that this new potential is highly homogeneous and could be used to study membrane peptides/proteins in micelles. We are currently using this potential to study the influence of the micellar environment on the structure and localization of transmembrane peptides originating from a large ABC membrane protein.[26]

■ ASSOCIATED CONTENT

Supporting Information

Force field parameters, charge values, as well as additional figures and tables. This material is available free of charge via the Internet at http://pubs.acs.org.

■ AUTHOR INFORMATION

Corresponding Author

*E-mail: stephane.abel@cea.fr.

Notes

The authors declare no competing financial interest.

■ ACKNOWLEDGMENTS

This work was, in part, granted access to the HPC resources of CCRT/CINES under the allocation t2011076076 made by GENCI (Grand Equipement National de Calcul Intensif). S.A. is grateful to Dr. D. Poger (University of Queensland, Brisbane, Australia) for providing the GROMOS54A7 parameters in the GROMACS format, Dr. Á. Piñeiro (University of Santiago de Compostela, Spain), and Dr. S. J. Marrink (University of Groningen, The Netherlands) for fruitful comments and pieces of advice about the results obtained in this work.

■ REFERENCES

(1) Arnold, T.; Linke, D. The use of detergents to purify membrane proteins. *Current Protocols in Protein Science*; 2008; Chapter 4, Units 53:4.8.1−4.8.30.

(2) Privé, G. Detergents for the stabilization and crystallization of membrane proteins. *Methods* **2007**, *41*, 388−397.

(3) Warschawski, D. E.; Arnold, A. A.; Beaugrand, M.; Gravel, A.; Chartrand, É.; Marcotte, I.; Chartrand, E. Choosing membrane mimetics for NMR structural studies of transmembrane proteins. *Biochim. Biophys. Acta: Biomembr.* **2011**, *1808*, 1957−1974.

(4) le Maire, M.; Champeil, P.; Moller, J. V.; Møller, J. V. Interaction of membrane proteins and lipids with solubilizing detergents. *Biochim. Biophys. Acta: Biomembr.* **2000**, *1508*, 86−111.

(5) Kallick, D. A.; Tessmer, M. R.; Watts, C. R.; Li, C. Y. The use of Dodecylphosphocholine micelles in solution NMR. *J. Magn. Reson. B* **1995**, *109*, 60−65.

(6) Gao, X. F.; Wong, T. C. Studies of the binding and structure of adrenocorticotropin peptides in membrane mimics by NMR spectroscopy and pulsed-field gradient diffusion. *Biophys. J.* **1998**, *74*, 1871−1888.

(7) de Foresta, B.; Vincent, M.; Garrigos, M.; Gallay, J. Transverse and tangential orientation of predicted transmembrane fragments 4 and 10 from the human multidrug resistance protein (hMRP1/ABCC1) in membrane mimics. *Eur. Biophys. J.* **2011**, *40*, 1043−1060.

(8) Dixon, A. M.; Venable, R. M.; Pastor, R. W.; Bull, T. E. Micelle-bound conformation of a hairpin-forming peptide: combined NMR and molecular dynamics study. *Biopolymers* **2002**, *65*, 284−298.

(9) Kim, H. J.; Howell, S. C.; Van Horn, W. D.; Jeon, Y. H.; Sanders, C. R. Recent Advances in the Application of Solution NMR Spectroscopy to Multi-Span Integral Membrane Proteins. *Prog. Nucl. Magn. Reson. Spectrosc.* **2009**, *55*, 335−360.

(10) Göbl, C.; Dulle, M.; Hohlweg, W.; Grossauer, J.; Falsone, S. F.; Glatter, O.; Zangger, K. Influence of phosphocholine alkyl chain length on peptide-micelle interactions and micellar size and shape. *J. Phys. Chem. B* **2010**, *114*, 4717−4724.

(11) Dike, A.; Cowsik, S. M. Solution structure of amphibian tachykinin perolein bound to DPC micelles. *J. Struct. Biol.* **2006**, *156*, 442−452.

(12) Bordag, N.; Keller, S. α-Helical transmembrane peptides: A "Divide and Conquer" approach to membrane proteins. *Chem. Phys. Lipids* **2010**, *163*, 1−26.

(13) Poget, S. F.; Girvin, M. E. Solution NMR of membrane proteins in bilayer mimics: small is beautiful, but sometimes bigger is better. *Biochim. Biophys. Acta* **2007**, *1768*, 3098−3106.

(14) Lauterwein, J.; Bösch, C.; Brown, L. R.; Wüthrich, K. Physicochemical studies of the protein-lipid interactions in melittin-containing micelles. *Biochim. Biophys. Acta: Biomembr.* **1979**, *556*, 244−264.

(15) Lipfert, J.; Columbus, L.; Chu, V. B.; Lesley, S. A.; Doniach, S. Size and shape of detergent micelles determined by small-angle X-ray scattering. *J. Phys. Chem. B* **2007**, *111*, 12427−12438.

(16) Wymore, T.; Gao, X. F.; Wong, T. C. Molecular dynamics simulation of the structure and dynamics of a dodecylphosphocholine micelle in aqueous solution. *THEOCHEM* **1999**, *485−486*, 195−210.

(17) Marrink, S.-J.; Tieleman, P. D.; Mark, A. E. Molecular Dynamics Simulation of the Kinetics of Spontaneous Micelle Formation. *J. Phys. Chem. B* **2000**, *104*, 12165−12173.

(18) Tieleman, D. P.; van der Spoel, D.; Berendsen, H. J. C. Molecular Dynamics Simulations of Dodecylphosphocholine Micelles at Three Different Aggregate Sizes: Micellar Structure and Chain Relaxation. *J. Phys. Chem. B* **2000**, *104*, 6380−6388.

(19) Vasudevan, S. V.; Balaji, P. V. Dynamics of Ganglioside Headgroup in Lipid Environment: Molecular Dynamics Simulations of GM1 Embedded in Dodecylphosphocholine Micelle. *J. Phys. Chem. B* **2001**, *105*, 7033−7041.

(20) Stephenson, B. C.; Goldsipe, A.; Beers, K. J.; Blankschtein, D. Quantifying the Hydrophobic Effect. 2. A Computer Simulation-Molecular-Thermodynamic Model for the Micellization of Nonionic

Surfactants in Aqueous Solution. *J. Phys. Chem. B* **2007**, *111*, 1045−1062.
(21) Marrink, S.-J.; de Vries, A. H.; Mark, A. E. Coarse Grained Model for Semi quantitative Lipid Simulations. *J. Phys. Chem. B* **2004**, *108*, 750−760.
(22) Fuzo, C. A.; Castro, J. R. M.; Degreve, L. Study of the antimicrobial peptide indolicidin and a mutant in micelle medium by molecular dynamics simulation. *Genet. Mol. Res.* **2008**, *7*, 986−999.
(23) Lazaridis, T.; Mallik, B.; Y., C.; Chen, Y. Implicit Solvent Simulations of DPC Micelle Formation. *J. Phys. Chem. B* **2005**, *109*, 15098−15106.
(24) Gouin, S.; Vanquelef, E.; Garcia Fernandez, J. M.; Ortiz Mellet, C.; Dupradeau, F.-Y.; Kovensky, J. Multi-Mannosides Based on a Carbohydrate Scaffold; Synthesis, Force Field Development, Molecular Dynamics Studies, and Binding Affinities for Lectin Con A. *J. Org. Chem.* **2007**, *72*, 9032−9045.
(25) Dupradeau, F.-Y.; Pigache, A.; Zaffran, T.; Savineau, C.; Lelong, R.; Grivel, N.; Lelong, D.; Rosanski, W.; Cieplak, P. The R.E.D. tools: advances in RESP and ESP charge derivation and force field library building. *Phys. Chem. Chem. Phys.* **2010**, *12*, 7821−7839.
(26) Abel, S.; Lorieau, A.; de Foresta, B.; Dupradeau, F.-Y.; Marchi, M. Molecular dynamics simulations of hMRP1 transmembrane segments in different environments. Manuscript in preparation, 2012.
(27) Hornak, V.; Abel, R.; Okur, A.; Strockbine, B.; Roitberg, A.; Simmerling, C. Comparison of multiple Amber force fields and development of improved protein backbone parameters. *Proteins Struct. Funct.* **2006**, *65*, 712−725.
(28) Jämbeck, J. P. M.; Lyubartsev, A. P. Derivation and systematic validation of a refined all-atom force field for phosphatidylcholine lipids. *J. Phys. Chem. B* **2012**, *116*, 3164−3179.
(29) Jämbeck, J. P. M.; Lyubartsev, A. P. An Extension and Further Validation of an All-Atomistic Force Field for Biological Membranes. *J. Chem. Theory Comput.* **2012**, *8*, 2938−2948.
(30) Dickson, C. J.; Rosso, L.; Betz, R. M.; Walker, R. C.; Gould, I. R. GAFFlipid: a General Amber Force Field for the accurate molecular dynamics simulation of phospholipid. *Soft Matter* **2012**, *8*, 9617−9627.
(31) Siu, S. W. I.; Vácha, R.; Jungwirth, P.; Böckmann, R. A. Biomolecular simulations of membranes: physical properties from different force fields. *J. Chem. Phys.* **2008**, *128*, 125103.
(32) Jójárt, B.; Martinek, T. A. Performance of the general amber force field in modeling aqueous POPC membrane bilayers. *J. Comput. Chem.* **2007**, *28*, 2051−2058.
(33) Klauda, J. B.; Venable, R. M.; Freites, J. A.; O'Connor, J. W.; Tobias, D. J.; Mondragon-Ramirez, C.; Vorobyov, I.; MacKerell, A. D.; Pastor, R. W. Update of the CHARMM All-Atom Additive Force Field for Lipids: Validation on Six Lipid Types. *J. Phys. Chem. B* **2010**, *114*, 7830−7843.
(34) Abel, S.; Dupradeau, F.-Y.; Raman, E. P.; MacKerell, A. D.; Marchi, M. Molecular simulations of dodecyl-β-maltoside micelles in water: influence of the headgroup conformation and force field parameters. *J. Phys. Chem. B* **2011**, *115*, 487−499.
(35) Kirschner, K. N.; Yongye, B., A.; Tschampel, M., S.; González-Outeiriño, J.; Daniels, R., C.; Lachele Foley, B.; J. Woods, R.; Kirschner, K.; Yongye, A.; Tschampel, S.; Daniels, C. GLYCAM06: A generalizable biomolecular force field. Carbohydrates. *J. Comput. Chem.* **2008**, *29*, 622−655.
(36) Cornell, W. D.; Cieplak, P.; Bayly, C. I.; Gould, I. R.; Merz, K. M.; Ferguson, D. M.; Spellmeyer, D. C.; Fox, T.; Caldwell, J. W.; Kollman, P. A. A Second Generation Force Field for the Simulation of Proteins, Nucleic Acids, and Organic Molecules. *J. Am. Chem. Soc.* **1995**, *117*, 5179−5197.
(37) Cheatham, T. E., III; Kollman, P. A. Molecular dynamics simulations of nucleic acids. *Annu. Rev. Phys. Chem.* **2000**, *51*, 435−471.
(38) Wang, J.; Wolf, R. M.; Caldwell, J. W.; Kollman, P. A.; Case, D. A. Development and testing of a general amber force field. *J. Comput. Chem.* **2004**, *25*, 1157−11574.
(39) Guvench, O.; MacKerell, A. D. Comparison of protein force fields for molecular dynamics simulations. *Methods Mol. Biol.* **2008**, *443*, 63−88.
(40) Cézard, C.; Trivelli, X.; Aubry, F.; Djedaïni-Pilard, F.; Dupradeau, F.-Y. Molecular dynamics studies of native and substituted cyclodextrins in different media: 1. Charge derivation and force field performances. *Phys. Chem. Chem. Phys.* **2011**, *13*, 15103−15121.
(41) Bayly, C. I.; Cieplak, P.; Cornell, W. D.; Kollman, P. A. A well-behaved electrostatic potential based method using charge restraints for deriving atomic charges: the RESP model. *J. Phys. Chem.* **1993**, *97*, 10269−10280.
(42) Cieplak, P.; Cornell, W. D.; Bayly, C.; Kollman, P. A. Application of the multimolecule and multiconformational RESP methodology to biopolymers: Charge derivation for DNA, RNA, and proteins. *J. Comput. Chem.* **1995**, *16*, 1357−1377.
(43) Dupradeau, F.-Y.; Cézard, C.; Lelong, R.; Stanislawiak, É.; Pêcher, J.; Delepine, J. C. R.E.DD.B.: A database for RESP and ESP atomic charges, and force field libraries. *Nucleic Acids Res.* **2008**, D360−D367.
(44) Hehre, W. J.; Radom, L.; Schleyer, P. V.; Pople, J. *Ab Initio Molecular Orbital Theory*; John Wiley and Sons: New York, 1986; p 576.
(45) Frisch, M. J. G.; Trucks, W.; Schlegel, H. B.; Scuseria, G. E.; Robb, M. A.; Cheeseman, J. R.; Scalmani, G.; Barone, V.; Mennucci, B.; Petersson, G. A.; Nakatsuji, H.; Caricato, M.; Li, X.; Hratchian, H. P.; Izmaylov, A. F.; Bloino, J.; Zheng, G.; Sonnenberg, J. L. *Gaussian 09*, Revision A.1; Gaussian, Inc: Wallingford, CT, 2009.
(46) Connolly, M. L. Analytical molecular surface calculation. *J. Appl. Crystallogr.* **1983**, *16*, 548−558.
(47) Vanquelef, E.; Simon, S.; Marquant, G.; Garcia, E.; Klimerak, G.; Delepine, J. C.; Cieplak, P.; Dupradeau, F.-Y. R.E.D. Server: a web service for deriving RESP and ESP charges and building force field libraries for new molecules and molecular fragments. *Nucleic Acids Res.* **2011**, *39*, W511−W517.
(48) Oostenbrink, C.; Soares, T. A.; van der Vegt, N. F. A.; van Gunsteren, W. F. Validation of the 53A6 GROMOS force field. *Eur. Biophys. J.* **2005**, *34*, 273−284.
(49) Poger, D.; Van Gunsteren, W. F.; Mark, A. E. A new force field for simulating phosphatidylcholine bilayers. *J. Comput. Chem.* **2010**, *31*, 1117−1125.
(50) Schmid, N.; Eichenberger, A. P.; Choutko, A.; Riniker, S.; Winger, M.; Mark, A. E.; van Gunsteren, W. F. Definition and testing of the GROMOS force-field versions 54A7 and 54B7. *Eur. Biophys. J.* **2011**, *40*, 843−856.
(51) Berger, O.; Edholm, O.; Jähnig, F. Molecular dynamics simulations of a fluid bilayer of dipalmitoylphosphatidylcholine at full hydration, constant pressure, and constant temperature. *Biophys. J.* **1997**, *72*, 2002−2013.
(52) Jorgensen, W. L.; Tirado-Rives, J. The OPLS [optimized potentials for liquid simulations] potential functions for proteins, energy minimizations for crystals of cyclic peptides and crambin. *J. Am. Chem. Soc.* **1988**, *110*, 1657−1666.
(53) Cordomí, A.; Perez, J. J. Molecular dynamics simulations of rhodopsin in different one-component lipid bilayers. *J. Phys. Chem. B* **2007**, *111*, 7052−7063.
(54) Monticelli, L.; Simões, C.; Belvisi, L.; Colombo, G. Assessing the influence of electrostatic schemes on molecular dynamics simulations of secondary structure forming peptides. *J. Phys.: Condens. Matter* **2006**, *18*, S329−S345.
(55) Chakrabarti, N.; Neale, C.; Payandeh, J.; Pai, E. F.; Pomès, R. An iris-like mechanism of pore dilation in the CorA magnesium transport system. *Biophys. J.* **2010**, *98*, 784−792.
(56) Piñeiro, Á.; Bond, P. J.; Khalid, S. Exploring the conformational dynamics and membrane interactions of PorB from C. glutamicum: a multi-scale molecular dynamics simulation study. *Biochim. Biophys. Acta* **2011**, *1808*, 1746−1752.
(57) Schwaiger, C. S.; Bjelkmar, P.; Hess, B.; Lindahl, E. 3pi-helix conformation facilitates the transition of a voltage sensor S4 segment toward the down state. *Biophys. J.* **2011**, *100*, 1446−1454.

(58) Bjelkmar, P.; Larsson, P.; Cuendet, M. A.; Hess, B.; Lindahl, E. Implementation of the CHARMM Force Field in GROMACS: Analysis of Protein Stability Effects from Correction Maps, Virtual Interaction Sites, and Water Models. *J. Chem. Theory Comput.* **2010**, *6*, 459−466.
(59) Sorin, E. J.; Pande, V. S. Empirical force-field assessment: The interplay between backbone torsions and noncovalent term scaling. *J. Comput. Chem.* **2005**, *26*, 682−690.
(60) Chiu, S. W.; Clark, M.; Balaji, V.; Subramaniam, S.; Scott, H. L.; Jakobsson, E. Incorporation of surface tension into molecular dynamics simulation of an interface: a fluid phase lipid bilayer membrane. *Biophys. J.* **1995**, *69*, 1230−1245.
(61) Van Der Spoel, D.; Lindahl, E.; Hess, B.; Groenhof, G.; Mark, A. E.; Berendsen, H. J. C. GROMACS: fast, flexible, and free. *J. Comput. Chem.* **2005**, *26*, 1701−18.
(62) Hess, B.; Kutzner, C.; van der Spoel, D.; Lindahl, E. GROMACS 4: Algorithms for Highly Efficient, Load-Balanced, and Scalable Molecular Simulation. *J. Chem. Theory Comput.* **2008**, *4*, 435−447.
(63) de Haas, G. H.; Bonsen, P. P.; Pieterson, W. A.; van Deenen, L. L. Studies on phospholipase A and its zymogen from porcine pancreas. 3. Action of the enzyme on short-chain lecithins. *Biochim. Biophys. Acta* **1971**, *239*, 252−266.
(64) Bond, P. J.; Sansom, M. S. P. Insertion and Assembly of Membrane Proteins via Simulation. *J. Am. Chem. Soc.* **2006**, *128*, 2697−2704.
(65) Bond, P. J.; Cuthbertson, J. M.; Deol, S. S.; Sansom, M. S. P. MD Simulations of Spontaneous Membrane Protein/Detergent Micelle Formation. *J. Am. Chem. Soc.* **2004**, *126*, 15948−15949.
(66) Khandelia, H.; Kaznessis, Y. N. Molecular Dynamics Simulations of the Helical Antimicrobial Peptide Ovispirin-1 in a Zwitterionic Dodecylphosphocholine Micelle: Insights into Host-Cell Toxicity. *J. Phys. Chem. B* **2005**, *109*, 12990−12996.
(67) Stephenson, B. C.; Goldsipe, A.; Blankschtein, D. Molecular Dynamics Simulation and Thermodynamic Modeling of the Self-Assembly of the Triterpenoids Asiatic Acid and Madecassic Acid in Aqueous Solution. *J. Phys. Chem. B* **2008**, *112*, 2357−2371.
(68) Chen, R.; Mark, A. E. The effect of membrane curvature on the conformation of antimicrobial peptides: implications for binding and the mechanism of action. *Eur. Biophys. J.* **2011**, *40*, 545−553.
(69) Jorgensen, W. L.; Chandrasekhar, J.; Madura, J. D.; Impey, R. W.; Klein, M. L. Comparison of simple potential functions for simulating liquid water. *J. Chem. Phys.* **1983**, *79*, 926−935.
(70) Berendsen, H. J. C.; Postma, J. P. M.; van Gunsteren, W. F. In *Intermolecular Forces*; Pullman, B., Ed.: Reider: Dodrecht, 1981; p 331.
(71) Miyamoto, S.; Kollman, P. A. Settle: An analytical version of the SHAKE and RATTLE algorithm for rigid water models. *J. Comput. Chem.* **1992**, *13*, 952−962.
(72) Bussi, G.; Donadio, D.; Parrinello, M. Canonical sampling through velocity rescaling. *J. Chem. Phys.* **2007**, *126*, 14101−14107.
(73) Rahman, A.; Stillinger, F. H. Molecular Dynamics Study of Liquid Water. *J. Chem. Phys.* **1971**, *55*, 3336−3359.
(74) Parrinello, M.; Rahman, A. Polymorphic transitions in single crystals: A new molecular dynamics method. *J. Appl. Phys.* **1981**, *52*, 7182−7190.
(75) Nosé, S. A molecular dynamics method for simulations in the canonical ensemble. *Mol. Phys.* **1984**, *52*, 255−268.
(76) Hoover, W. G. Canonical dynamics: Equilibrium phase-space distributions. *Phys. Rev. A* **1985**, *31*, 1695−1697.
(77) Essmann, U.; Perera, L.; Berkowitz, M. L.; Darden, T.; Lee, H.; Pedersen, L. G. A smooth particle mesh Ewald method. *Chem. Phys.* **1995**, *103*, 8577−8594.
(78) Tironi, I. G.; Sperb, R.; Smith, P. E.; van Gunsteren, W. F. A generalized reaction field method for molecular dynamics simulations. *J. Chem. Phys.* **1995**, *102*, 5451−5459.
(79) Lange, O. F.; van der Spoel, D.; de Groot, B. L. Scrutinizing Molecular Mechanics Force Fields on the Submicrosecond Timescale with NMR Data. *Biochem. J.* **2010**, *99*, 647−655.
(80) Hess, B. P-LINCS: A Parallel Linear Constraint Solver for Molecular Simulation. *J. Chem. Theory Comput.* **2007**, *4*, 116−122.
(81) Sanders, S. A.; Sammalkorpi, M.; Panagiotopoulos, A. Z. Atomistic simulations of micellization of sodium hexyl, heptyl, octyl, and nonyl sulfates. *J. Phys. Chem. B* **2012**, *116*, 2430−2437.
(82) Maillet, J.-B.; Lachet, V.; Coveney, P. V. Large scale molecular dynamics simulation of self-assembly processes in short and long chain cationic surfactants. *Phys. Chem. Chem. Phys.* **1999**, *1*, 5277−5290.
(83) Abel, S.; Attia, J.; Rémita, S.; Marchi, M.; Urbach, W.; Goldmann, M. Atomistic simulations of spontaneous formation and structural properties of linoleic acid micelles in water. *Chem. Phys. Lett.* **2009**, *481*, 124−129.
(84) Turner, D. C.; Yin, F.; Kindt, J. T.; Zhang, H. Molecular Dynamics Simulations of Glycocholate−Oleic Acid Mixed Micelle Assembly. *Langmuir* **2010**, *26*, 4687−4692.
(85) Jusufi, A.; Hynninen, A.-P.; Panagiotopoulos, A. Z. Implicit Solvent Models for Micellization of Ionic Surfactants. *J. Phys. Chem. B* **2008**, *112*, 13783−13792.
(86) Jorgensen, W. L.; Maxwell, D. S.; Tirado-Rives, J. Development and Testing of the OPLS All-Atom Force Field on Conformational Energetics and Properties of Organic Liquids. *J. Am. Chem. Soc.* **1996**, *118*, 11225−11236.
(87) Jorge, M. Molecular dynamics simulation of self-assembly of n-decyltrimethylammonium bromide micelles. *Langmuir* **2008**, *24*, 5714−25.
(88) Nyrkova, I. A.; Semenov, A. N. On the Theory of Micellization Kinetics. *Macromol. Theory Simul.* **2005**, *14*, 569−585.
(89) Zhang, J.; Liu, S. Kinetics of thermo-induced micelle-to-vesicle transitions in a catanionic surfactant system investigated by stopped-flow temperature jump. *Phys. Chem. Chem. Phys.* **2011**, *13*, 12545−12553.
(90) Marchi, M. trjVoronoi, is a computational tool written in C++, which uses the voro++ library (version 0.4.3) of C. H. Rycroft to implement the Voronoi tessellation for frames of a GROMACS trajectory. It can compute the Voronoi volume of any given atoms. It can be downloaded from http://trjvoronoi-cplusplus.googlecode.com/files/trjVoronoi-06-07-2012.tgz.
(91) Rycroft, C. H. VORO++: a three-dimensional voronoi cell library in C++. *Chaos* **2009**, *19*, 041111.
(92) Voronoi, G. F. Nouvelles applications des paramètres continus à la théorie des formes quadratiques. *J. Reine Angew. Math.* **1908**, *134*, 198−287.
(93) Voloshin, V. P.; Medvedev, N. N.; Andrews, M. N.; Burri, R. R.; Winter, R.; Geiger, A. Volumetric properties of hydrated peptides: Voronoi-Delaunay analysis of molecular simulation runs. *J. Phys. Chem. B* **2011**, *115*, 14217−14228.
(94) Paci, E.; Marchi, M. Intrinsic compressibility and volume compression in solvated proteins by molecular dynamics simulation at high pressure. *Proc. Natl. Acad. Sci. U.S.A.* **1996**, *93*, 11609−11614.
(95) Bruce, C. D.; Berkowitz, M. L.; Perera, L.; Forbes, M. D. E. Molecular Dynamics Simulation of Sodium Dodecyl Sulfate Micelle in Water: Micellar Structural Characteristics and Counterion Distribution. *J. Phys. Chem. B* **2002**, *106*, 3788−3793.
(96) Aicart, E.; Tardajos, G.; Diaz Pena, M. Isothermal compressibility of cyclohexane-n-decane, cyclohexane-n-dodecane, and cyclohexane-n-tetradecane. *J. Chem. Eng. Data* **1981**, *26*, 22−26.
(97) Rossini, F. D. In *Selected Values of physical Thermodynamic Properties of Hydrocarbons and Related Compounds*; Carnegie, P., Ed.; American Petroleum Institute: Pittsburgh, PA, 1953; 1050 pages.
(98) Yaseen, M.; Lu, J. R.; Webster, J. R. P.; Penfold, J. The structure of zwitterionic phosphocholine surfactant monolayers. *Langmuir* **2006**, *22*, 5825−5832.
(99) Brumm, T.; Naumann, C.; Sackmann, E.; Rennie, A. R.; Thomas, R. K.; Kanellas, D.; Penfold, J.; Bayerl, T. M. Conformational changes of the lecithin headgroup in monolayers at the air/water interface. *Eur. Biophys. J.* **1994**, *23*, 289−295.
(100) Johnson, S. J.; Bayerl, T. M.; McDermott, D. C.; Adam, G. W.; Rennie, A. R.; Thomas, R. K.; Sackmann, E. Structure of an adsorbed dimyristoylphosphatidylcholine bilayer measured with specular reflection of neutrons. *Biophys. J.* **1991**, *59*, 289−294.

(101) Kucerka, N.; Kiselev, M. A.; Balgavý, P. Determination of bilayer thickness and lipid surface area in unilamellar dimyristoylphosphatidylcholine vesicles from small-angle neutron scattering curves: a comparison of evaluation methods. *Eur. Biophys. J.* **2004**, *33*, 328−334.
(102) Schrodinger LLC. *The PyMOL Molecular Graphics System*, Version 1.3r1; DeLano Scientific: San Carlos, CA, 2010.
(103) Seelig, J.; Gally, H.-U.; Wohlgemuth, R. Orientation and flexibility of the choline head group in phosphatidylcholine bilayers. *Biochim. Biophys. Acta* **1977**, *467*, 109−119.
(104) Eisenhaber, F.; Lijnzaad, P.; Argos, P.; Sander, C.; Scharf, M. The double cubic lattice method: Efficient approaches to numerical integration of surface area and volume and to dot surface contouring of molecular assemblies. *J. Comput. Chem.* **1995**, *16*, 273−284.
(105) Tsai, J.; Taylor, R.; Chothia, C.; Gerstein, M. The packing density in proteins: standard radii and volumes. *J. Mol. Biol.* **1999**, *290*, 253−266.
(106) Poger, D.; Mark, A. E. Turning the growth hormone receptor on: evidence that hormone binding induces subunit rotation. *Proteins* **2010**, *78*, 1163−1174.
(107) Foglia, F.; Lawrence, M. J.; Lorenz, C. D.; McLain, S. E. On the hydration of the phosphocholine headgroup in aqueous solution. *J. Chem. Phys.* **2010**, *133*, 145103.
(108) Lopez, C. F.; Nielsen, S. O.; Klein, M. L.; Moore, P. B. Hydrogen Bonding Structure and Dynamics of Water at the Dimyristoylphosphatidylcholine Lipid Bilayer Surface from a Molecular Dynamics Simulation. *J. Phys. Chem. B* **2004**, *108*, 6603−6610.
(109) Tieleman, P. D.; Berendsen, H. J. C. Molecular dynamics simulations of a fully hydrated dipalmitoylphosphatidylcholine bilayer with different macroscopic boundary conditions and parameters. *J. Chem. Phys.* **1996**, *105*, 4871.
(110) Murzyn, K.; Róg, T.; Jezierski, G.; Takaoka, Y.; Pasenkiewicz-Gierula, M. Effects of phospholipid unsaturation on the membrane/water interface: a molecular simulation study. *Biophys. J.* **2001**, *81*, 170−183.
(111) Pasenkiewicz-Gierula, M.; Takaoka, Y.; Miyagawa, H.; Kitamura, K.; Kusumi, A. Hydrogen Bonding of Water to Phosphatidylcholine in the Membrane As Studied by a Molecular Dynamics Simulation: Location, Geometry, and Lipid−Lipid Bridging via Hydrogen-Bonded Water. *J. Phys. Chem. A* **1997**, *101*, 3677−3691.
(112) Hauser, H.; Guyer, W.; Pascher, I.; Skrabal, P.; Sundell, S. Polar group conformation of phosphatidylcholine. Effect of solvent and aggregation. *Biochemistry* **1980**, *19*, 366−373.
(113) Krishnamurty, S.; Stefanov, M.; Mineva, T.; Bégu, S.; Devoisselle, J. M.; Goursot, A.; Zhu, R.; Salahub, D. R. Density functional theory-based conformational analysis of a phospholipid molecule (dimyristoyl phosphatidylcholine). *J. Phys. Chem. B* **2008**, *112*, 13433−13442.
(114) Pandey, P. R.; Roy, S. Headgroup mediated water insertion into the DPPC bilayer: a molecular dynamics study. *J. Phys. Chem. B* **2011**, *115*, 3155−3163.
(115) Akutsu, H.; Nagamori, T. Conformational analysis of the polar head group in phosphatidylcholine bilayers: a structural change induced by cations. *Biochemistry* **1991**, *30*, 4510−4516.
(116) Holler, F.; Callis, J. B. Conformation of the hydrocarbon chains of sodium dodecyl sulfate molecules in micelles: an FTIR study. *J. Phys. Chem.* **1989**, *93*, 2053−2058.
(117) Klauda, J. B.; Brooks, B. R.; MacKerell, A. D.; Venable, R. M. R. M.; Pastor, R. W.; MacKerell, A. D., Jr. An ab initio study on the torsional surface of alkanes and its effect on molecular simulations of alkanes and a DPPC bilayer. *J. Phys. Chem. B* **2005**, *109*, 5300−5311.
(118) Feller, S. E.; Zhang, Y.; Brooks, B. R. Constant pressure molecular dynamics simulation: The Langevin piston method. *J. Chem. Phys.* **1995**, *103*, 4613−4621.
(119) MacKerell, A. D., Jr. Molecular Dynamics Simulation Analysis of a Sodium Dodecyl Sulfate Micelle in Aqueous Solution: Decreased Fluidity of the Micelle Hydrocarbon Interior. *J. Phys. Chem.* **1995**, *99*, 1846−1855.
(120) Bogusz, S.; Venable, R.; Pastor, R. W. Molecular Dynamics Simulations of Octyl Glucoside Micelles: Structural Properties. *J. Phys. Chem. B* **2000**, *104*, 5462−5470.
(121) Sterpone, F.; Briganti, G.; Pierleoni, C. Molecular Dynamics Study of Spherical Aggregates of Chain Molecules at Different Degrees of Hydrophilicity in Water Solution. *Langmuir* **2001**, *17*, 5103−5110.
(122) Marchetti, G.; Marchi, M.; Le Maire, M. Modélisation moléculaire du phénomène du transport du calcium dans la protéine ATPAse-Ca2+ (SERCA1a). Ph.D. Thesis, 2006, p 165.
(123) Borle, F.; Seelig, J. Hydration of Escherichia coli lipids. *Biochim. Biophys. Acta Biomembr.* **1983**, *735*, 131−136.